THE JOURNAL OF BIOLOGICAL CHEMISTRY VOL. 284, NO. 46, pp. 31789–31797, November 13, 2009

Ferredoxin:NADP$^+$ Oxidoreductase Association with Phycocyanin Modulates Its Properties*[S]

Received for publication, May 23, 2009, and in revised form, September 11, 2009 Published, JBC Papers in Press, September 15, 2009, DOI 10.1074/jbc.M109.024638

Anja Korn, Ghada Ajlani[1], Bernard Lagoutte, Andrew Gall, and Pierre Sétif[2]

From the Institut de Biologie et de Technologie de Saclay, Commissariat à L'Energie Atomique, CNRS, F-91191 Gif sur Yvette, France

In photosynthetic organisms, ferredoxin:NADP$^+$ oxidoreductase (FNR) is known to provide NADPH for CO_2 assimilation, but it also utilizes NADPH to provide reduced ferredoxin. The cyanobacterium *Synechocystis* sp. strain PCC6803 produces two FNR isoforms, a small one (FNR_S) similar to the one found in plant plastids and a large one (FNR_L) that is associated with the phycobilisome, a light-harvesting complex. Here we show that a mutant lacking FNR_L exhibits a higher NADP$^+$/NADPH ratio. We also purified to homogeneity a phycobilisome subcomplex comprising FNR_L, named FNR_L-PC. The enzymatic activities of FNR_L-PC were compared with those of FNR_S. During NADPH oxidation, FNR_L-PC exhibits a 30% decrease in the Michaelis constant $K_{m(NADPH)}$, and a 70% increase in $K_{m(ferredoxin)}$, which is in agreement with its predicted lower activity of ferredoxin reduction. During NADP$^+$ reduction, the FNR_L-PC shows a 29/43% decrease in the rate of single electron transfer from reduced ferredoxin in the presence/absence of NADP$^+$. The increase in $K_{m(ferredoxin)}$ and the rate decrease of single reduction are attributed to steric hindrance by the phycocyanin moiety of FNR_L-PC. Both isoforms are capable of catalyzing the NADP$^+$ reduction under multiple turnover conditions. Furthermore, we obtained evidence that, under high ionic strength conditions, electron transfer from reduced ferredoxin is rate limiting during this process. The differences that we observe might not fully explain the *in vivo* properties of the *Synechocystis* mutants expressing only one of the isoforms. Therefore, we advocate that FNR localization and/or substrates availability are essential *in vivo*.

In cyanobacteria and plastids, ferredoxin:NADP$^+$ oxidoreductase (FNR)[3] catalyzes the exchange of electrons between the one-electron carrier ferredoxin (Fd) and the two-electron carrier NADP$^+$ (1–5): 2 Fd_{red} + NADP$^+$ + H$^+$ ⇆ 2 Fd_{ox} + NADPH. FNR contains the noncovalently bound FAD cofactor. The NADP$^+$-reductase catalytic cycle involves the reduction of FAD to the neutral semiquinone FADH$^\bullet$ (FNR_{sq}) followed by its further reduction to the fully reduced FADH$^-$ (FNR_{red}), with reduced Fd (Fd_{red}) binding at a single site (4, 6). Hydride transfer from FADH$^-$ to NADP$^+$ completes the catalytic cycle (7) and NADPH is then released. Ternary complexes between the three partners FNR, NADP$^+$ and Fd have been shown to be involved in NADP$^+$-reductase activity (1, 8). This is in line with the fact that fast turnover requires NADP$^+$ binding before Fd_{red} binding, FAD reduction, and Fd_{ox} release (1). Such ternary complexes may not be required during the NADPH-oxidase catalytic cycle (7, 9), although this has yet to be established. In the final step of linear photosynthetic electron flow, FNR is involved in NADPH production, which in turn is used in the Calvin cycle. In plant plastids several FNR isoforms are encoded by different genes (10–12). The expressed enzymes are processed to give molecular masses of ~35 kDa. The different isoforms are differentially expressed in roots and leaves (13). The root enzyme is involved in NADPH consumption, reducing Fd for nitrogen fixation, while the leaf enzyme is involved in NADPH formation (14–17).

The biochemical and structural properties of cyanobacterial and plastid FNR are highly similar except that in most phycobilisome (PBS)-containing cyanobacteria, FNR contains an N-terminal domain whose sequence is similar to PBS-linker polypeptides (18). This extension is responsible for FNR_L attachment to the PBS (18). The conventional PBS is composed of two substructures, the core and the rods. In *Synechocystis* sp. strain PCC6803 (hereafter named *Synechocystis*), the core is composed of allophycocyanin (AP) and each rod contains three phycocyanin (PC) discs. Different linkers are specifically responsible for each level of phycobiliprotein assembly and function to stabilize the PBS and optimize its absorption and energy transfer characteristics (19). FNR_L has been shown to bind to the PBS rods but its precise binding site is still controversial (20–22). Smaller FNR isoforms have been purified from several cyanobacteria and this was attributed to proteolytic degradation of the N-terminal domain (18, 23). However, it has been recently demonstrated that in *Synechocystis* the small isoform (FNR_S, ≈34 kDa) results from an internal translation initiation and not from proteolysis of the large isoform (24). The same authors proposed that FNR_L functions as an NADP$^+$ reductase whereas FNR_S is a better NADPH oxidase. More precisely, FNR_L was shown to support photoautotrophic growth in *Synechocystis* whereas it is the only isoform found in obligate

* This work was supported in part by the Agence Nationale de la Recherche, France (PHYCOSYN, to G. A. and ANR-07-CEXC-009, to A. G.) and the European Commission (EU FP7-ENERGY-2007-1-RTD SOLAR-H2, to P. S.).

[S] The on-line version of this article (available at http://www.jbc.org) contains supplemental Figs. S1 and S2 and Table S1.

[1] To whom correspondence may be addressed: CEA Saclay, iBiTecS, F-91191 Gif sur Yvette, France. Tel.: 33-169086569; Fax: 33-169088717; E-mail: gajlani@cea.fr.

[2] To whom correspondence may be addressed: CEA Saclay, iBiTecS, F-91191 Gif sur Yvette, France. Tel.: 33-169089867; Fax: 33-169088717; E-mail: pierre.setif@cea.fr.

[3] The abbreviations used are: FNR, ferredoxin:NADP$^+$ oxidoreductase; AP, allophycocyanin; α^{PC} and β^{PC}, the two subunits of phycocyanin; cyt *c*, cytochrome *c*; E_m, midpoint redox potential; Fd, ferredoxin; red, reduced; ox, oxidized; FNR_{sq}, singly reduced FNR/semiquinone form; FNR_S, small *Synechocystis* FNR isoform; FNR_L, large *Synechocystis* FNR isoform; PBS, phycobilisome; PC, phycocyanin, an $\alpha\beta$ protomer; PSI, photosystem I; P700, primary electron donor of photosystem I; *Synechocystis*, *Synechocystis* sp. PCC6803; L_{CM}, core-membrane linker; L_{RC}, rod-core linker.

phototrophic cyanobacteria. Conversely, FNR$_S$ accumulates when photosynthesis is slowed down, *i.e.* under heterotrophic or starvation conditions (24). These observations support the idea that the two isoforms differ in their $NADP^+$-reductase/NADPH-oxidase activities. This can be regarded as analogous to the leaf and root isoforms of plants.

Both *Synechocystis* isoforms being encoded by the same gene, they share identical catalytic domains. The N-terminal extension of FNR$_L$ or its association to PBS could somehow modify its catalytic properties. As FNR$_L$ is bound *in vivo* to the core-containing PBS and undergoes proteolysis when not bound to it (25), it is crucial to compare the enzymatic properties of FNR$_S$ to those of PBS-bound FNR$_L$. However, in practical terms, the large extinction coefficient of the PBS makes such experiments virtually impossible since they are based on absorption measurements. This was circumvented by the purification of a PBS subcomplex, termed FNR$_L$-PC that contained FNR$_L$, a PC hexamer and a PBS rod-core linker (L$_{RC}$). The FNR$_L$-PC complex possesses a lower extinction coefficient than that of the whole PBS and thus permits absorption measurements to be undertaken.

In this work, we established that the $NADP^+$/NADPH ratio is higher in a mutant containing only FNR$_S$. An FNR$_L$-PC complex was purified to homogeneity and shown to be stable for several days in 150 mM phosphate buffer. Finally, the catalytic activities and kinetic constants of the two FNR isoforms are compared with each other and to their plant homologues.

EXPERIMENTAL PROCEDURES

Materials—Synechocystis strains were grown at 34 °C in a CO_2 enriched atmosphere under 60 μE m^{-2} s^{-1} illumination in a modified Allen's medium (26). Photosystem I (PSI) was purified from *Synechocystis* wild type (27), whereas Fd, FNR$_S$, and FNR$_L$ were overexpressed in *Escherichia coli* and purified as previously described (5, 28). NADPH and horse-heart cytochrome *c* (cyt *c*) were purchased from Sigma-Aldrich. ProBond Ni-resin was obtained from Invitrogen. An antiprotease mixture (Complete, Roche Applied Sciences) was used during the isolation of FNR$_L$-PC.

$NADP^+$/NADPH Quantification—Absolute and relative amounts of pyridine nucleotides were obtained using an EnzyChrom™ $NADP^+$/NADPH assay kit (Gentaur, France) for the wild type and the two mutants where only one FNR isoform is expressed, *i.e.* FNR$_S$ and FNR$_L$ in the FS1 and MI6 mutants, respectively (24). These measurements were performed with cells in their exponential growth phase under photoautotrophic conditions.

Construction and Purification of His-tagged FNR$_L$ in Synechocystis—Because the N- and C-terminal domains of the enzyme are buried in the PC hexamer and the NADP binding site of the FNR, respectively, a His tag was inserted into the exposed hinge domain preceding the catalytic FNR$_S$ domain (Fig. 1). PCR mutagenesis was performed on the *petH* gene of *Synechocystis* to introduce 6 histidines (between Gly-98 and Ser-99). The mutagenic primers were HIF (5′-CCATCATCACCATCACTCAGGAGCGGTGGC-3′) and HIR (5′-GATGGTGATGATGGTGACCACTTCCCTCGG-3′). The overall method was similar to that used in Ref. 24. The modified gene was introduced in CB, a *Synechocystis* mutant that contains only one PC hexamer per rod instead of three as expressed in the wild type (26). The resulting strain was named CBH.

Phycobilisomes were purified from CBH under conditions that are known (29–31) to preserve PBS-subunit interactions, *i.e.* 0.8 M phosphate (KP: potassium phosphate buffer, pH 8.0). Membranes and chlorophylls were eliminated by Triton X-100 extraction. The PBS complex was then allowed to dissociate overnight at 4 °C by lowering the phosphate concentration to 150 mM KP. The sample was then added to a Ni-resin equilibrated in 250 mM KP and allowed to bind for 1 h. After two washes in the same buffer, the resin was poured into a column. After extensive washing with 150 mM KP, FNR$_L$ was eluted in the presence of 150 mM imidazole. The eluted fractions were concentrated using Vivaspin concentrators (100 kDa cut-off). For each fraction, the PC hexamer concentration was determined by absorption spectroscopy ($\epsilon_{620\ nm}$ = 2.37 μM^{-1} cm^{-1}, Ref. 32) prior to gel filtration chromatography (250 mM KP, 26/85 Superdex 200, GE Healthcare). Elution profiles were obtained by monitoring the absorbance at 280, 460, and 620 nm, which are indicative of the relative amounts of protein, FAD, and PC, respectively (supplemental Fig. S1). The polypeptide composition of each fraction was analyzed by SDS-PAGE. Polypeptide quantifications were achieved by measuring the Coomassie Blue density of the different bands using an Image scanner II (GE Healthcare). Different amounts of FNR$_L$-PC were loaded and the staining of the FNR$_L$ polypeptide was compared with known amounts of recombinant FNR$_L$ that were loaded in neighboring lanes.

Measurements of FAD Content in the FNR$_L$-PC Complex—The polypeptides of FNR$_L$-PC from three different batches were precipitated by the addition of trichloroacetic acid (5% w/v). Under these conditions, the released FAD cofactor is recovered in the supernatant (33). FAD concentrations were calculated from the absorption maxima at 450 nm ($\epsilon_{450\ nm}$ = 11,300 M^{-1} cm^{-1}, Ref. 34). This is illustrated in supplemental Fig. S2. In parallel, the pelleted polypeptides were solubilized for SDS-PAGE, and FNR$_L$ quantified after electrophoretic separation. These two approaches allowed us to compare the FNR$_L$ and FAD contents.

Determination of the Absorption Coefficients of FNR$_S$ and FNR$_L$—As detailed in supplemental data, the FAD cofactor from recombinant FNR$_S$ and FNR$_L$ was released and quantified in the presence of 0.02% SDS (w/v). This allowed us to reevaluate the absorption coefficients of both FNR isoforms. They were determined to be 9,000 M^{-1} cm^{-1} at 461 nm instead of 10,800 M^{-1} cm^{-1} that was previously reported for plant FNR (35).

Oxidase Activities—Enzymatic reactions were monitored with a Uvikon-XL spectrophotometer. The initial velocities were fitted with Origin 7.5 (OriginLab Corp., Northampton, MA) to obtain Henri-Michaelis-Menten curves. Ferricyanide reductase activity was measured at room temperature in duplicate with NADPH and potassium ferricyanide as the electron donor and acceptor molecules, respectively (36). A series of FNR$_S$/FNR$_L$-PC concentrations (0.025–0.1 μM) was mixed with 0.7 mM potassium ferricyanide and 5 mM $MgCl_2$ in 150 mM KP. The reactions were initiated by the addition of a range of

different NADPH concentrations (25–400 μM). The absorption decrease at 420 nm (reduction of ferricyanide) was recorded to determine the steady-state kinetic parameters.

The Fd-mediated cyt *c* reductase activity of FNR$_S$/FNR$_L$-PC was measured at 25 °C in triplicate with Fd and cyt *c* acting as intermediate and terminal electron acceptors (35, 36). The reaction was started by the addition of NADPH (400 μM final concentration). Steady-state kinetic parameters for the Fd-dependent cyt *c* reductase activity were determined by varying the concentrations of Fd (2.5–40 μM) in the reaction mixtures and monitoring the resulting absorption increases at 550 nm (reduction of cyt *c*). Fd from *Thermosynechococcus elongatus* was used for these experiments as it was available in large quantities. A few control measurements were performed with *Synechocystis* Fd giving results identical to those obtained with *T. elongatus* Fd.

Flash Absorption Experiments for the Measurements of Reductase Activities—Flash absorption measurements with a time resolution of 10 μs were performed as described previously (5) at 22 °C. Laser excitation (700 nm) was provided by a dye laser (Continuum, Excel Technology, Villebon sur Yvette, France) pumped by a frequency-doubled Nd-Yag laser and was saturating for PSI photochemistry. Conditions were chosen to eliminate any actinic effect of the measuring light.

All spectroscopic measurements were performed under aerobic conditions in 150 mM KP containing 30 mM NaCl and 0.03% (w/v) β-dodecyl maltoside (Biomol, Hamburg, Germany). Sodium ascorbate (2 mM) and 2.6-dichlorophenolindophenol (5–25 μM) were used to reduce the oxidized P700 between two consecutive flashes. The PSI concentration was estimated using the absorption coefficient $\epsilon_{800\ nm} = 7.74\ mM^{-1}\ cm^{-1}$ for $P700^+$ (5). For all flash experiments, the kinetics is shown after subtraction of the $P700^+$ contribution. This was achieved by measuring, in the absence of Fd, the differential absorption coefficients of $P700^+$ at 520/540 nm and at 800 nm, using methyl viologen as an electron acceptor that results in fast reoxidation of the terminal PSI acceptor $(F_A,F_B)^-$. Using this procedure, the differential absorption coefficient of $P700^+$ at 520/540 nm was found to be 50%/34% that of $P700^+$ at 800 nm ($\Delta\epsilon_{520\ nm} = 3.9\ mM^{-1}\ cm^{-1} \approx 7.74\ mM^{-1}\ cm^{-1} \times 0.50$; $\Delta\epsilon_{540\ nm} = 2.6\ mM^{-1}\ cm^{-1} \approx 7.74\ mM^{-1}\ cm^{-1} \times 0.34$). The kinetics probed at 800 nm was subtracted, after multiplication by the normalization factor of 0.50/0.34. In this way, all absorption changes are associated with the reduction of the electron acceptors, *i.e.* those due to (F_A, F_B), Fd, and FNR.

Single reduction of FNR by reduced Fd was triggered by flash excitation of PSI. These experiments were performed in the presence/absence of $NADP^+$ with FNR in excess over PSI. Under this condition, a single reduction event is favored where the neutral protonated semiquinone is produced. These measurements were performed at 520 nm, which corresponds to an absorption minimum of the PSI/FNR$_L$-PC mixture (Fd absorbance is small compared with those of PSI and PC). Moreover, a large signal is expected at 520 nm for formation of the FNR semireduced form FNR$_{sq}$.

To promote multiple catalytic turnover, the PSI concentration was >10-fold greater than that of the investigated enzyme (either FNR$_S$ or FNR$_L$-PC). Under these conditions, FNR receives two electrons from Fd and NADPH is formed via hydride transfer. This multiple turnover reaction was monitored by the reoxidation of Fd$_{red}$ at 540 nm. This wavelength was chosen because of the minimal PSI absorption, which allows actinic effects of the measuring light to be minimized in these measurements made on a long time scale (5).

Fittings and Calculations—The kinetic model used to interpret the single FNR reduction experiments is shown under "Results." It involves two reactions, the first one describes Fd reduction by PSI and the second one corresponds to the redox equilibrium of the first FNR reduction by Fd$_{red}$. Such a model does not take into account complex formation and dissociation, because of the large ionic strength of the medium, which impedes formation of complexes (2, 37) and hence only considers second-order processes. We assume also that the PSI charge separation leading to the formation of $(F_A, F_B)^-$ is much faster than the subsequent steps since it occurs in the submicrosecond range (38). The kinetic analysis is further simplified as the experiments were performed under conditions where one partner is in large excess over the other one for each of the reactions: $[Fd_{ox}] \gg [PSI_{red}]$, $[FNR_{ox}] \gg [Fd_{red}]$, $[Fd_{ox}] \gg [FNR_{sq}]$. This allows the system of time-differential equations corresponding to the model to be solved analytically, using the three following first-order rate Equations 1–3,

$$k_{rFd} = k_r \times [Fd] \quad \text{(Eq. 1)}$$

with [Fd] as the total Fd concentration ($[Fd_{red}] \ll [Fd_{ox}]$),

$$k_{red} = k_1 \times [FNR] \quad \text{(Eq. 2)}$$

with [FNR] as the total FNR concentration ($[FNR_{sq}] \ll [FNR_{ox}]$).

$$k_{ox} = k_{-1} \times [Fd] \quad \text{(Eq. 3)}$$

The solution is then shown in Equations 4–6,

$$[PSI_{red}](t) = [PSI] \times e^{-k_{rFd}t} \quad \text{(Eq. 4)}$$

$$[Fd_{red}](t) = [PSI] \times \left[\frac{k_{rFd} - k_{ox}}{k_{ox} + k_{red} - k_{rFd}} \times e^{-k_{rFd}t} - \frac{k_{red}k_{rFd}}{(k_{ox} + k_{red} - k_{rFd})(k_{ox} + k_{red})} \times e^{-(k_{ox} + k_{red})t} + \frac{k_{ox}}{k_{ox} + k_{red}} \right] \quad \text{(Eq. 5)}$$

$$[FNR_{sq}](t) = [PSI] \times \left[\frac{-k_{red}}{k_{ox} + k_{red} - k_{rFd}} \times e^{-k_{rFd}t} + \frac{k_{red}k_{rFd}}{(k_{ox} + k_{red} - k_{rFd})(k_{ox} + k_{red})} \times e^{-(k_{ox} + k_{red})t} + \frac{k_{red}}{k_{ox} + k_{red}} \right] \quad \text{(Eq. 6)}$$

with [PSI] as the total PSI concentration. The Excel solver (V. 2003, Microsoft) was used to fit the experimental results with the above equations.

When measuring multiple turnover event from reoxidation of Fd$_{red}$, the decay kinetics were able to be fitted with a single exponential component (5). The initial decay rate k_{noFNR} in the absence

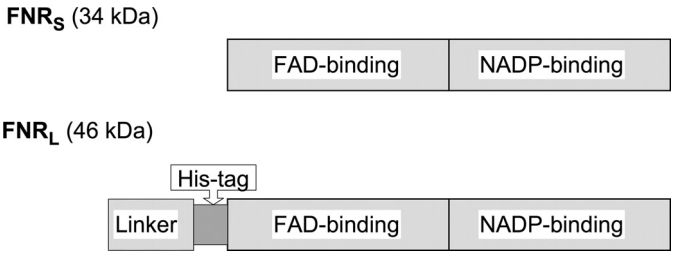

FIGURE 1. **Representation of the FNR primary structures highlighting their functional domains.** FNR$_S$ is restricted to the catalytic part that is divided into the FAD binding domain and the NADP binding domain. FNR$_L$ contains an N-terminal extension that comprises the PBS-linker domain and a hinge domain, whose length and primary sequence are variable depending on the cyanobacterium. Because the N- and C-terminal domains of the enzyme are buried in the PBS and the NADP binding site, respectively, the His tag was inserted into the hinge domain.

of FNR was subtracted from the exponential rate k_{FNR} in its presence. The initial turnover rate was then calculated from Equation 7,

$$-(d[Fd_{red}]/dt)_{t=0}/[FNR] = (k_{FNR} - k_{noFNR}) \times [PSI]/[FNR] \quad \text{(Eq. 7)}$$

as $[PSI] = [Fd_{red}]_{t=0}$.

This rate can also be calculated from rate k_1 of Reaction 2 (see "Results") when this reaction is rate limiting. From Reaction 2, the decay rate of Fd_{red} is shown in Equation 8,

$$d[Fd_{red}]/dt = -k_1[Fd_{red}][FNR_{ox}] + k_{-1}[Fd_{ox}][FNR_{sq}] \quad \text{(Eq. 8)}$$

which gives, for $t = 0$, Equation 9,

$$(d[Fd_{red}]/dt)_{t=0} = -k_1[Fd_{red}]_{t=0}[FNR] \quad \text{(Eq. 9)}$$

with [FNR] as the total concentration of FNR. With $[PSI] = [Fd_{red}]_{t=0}$ one gets Equation 10.

$$-(d[Fd_{red}]/dt)_{t=0}/[FNR] = k_1[PSI] \quad \text{(Eq. 10)}$$

RESULTS

Quantification of NADP$^+$ and NADPH in Cell Extracts—The cellular contents of NADP$^+$ and NADPH were measured in three *Synechocystis* strains grown under photoautotrophic conditions, the wild type and two mutants containing only one of the FNR isoforms, *i.e.* FNR$_L$ and FNR$_S$ in MI6 and FS1, respectively (24). The NADP$^+$/NADPH ratios were 2.6 ± 0.2, 2.0 ± 0.4, and 4.3 ± 0.8 for the wild type, MI6, and FS1 strains, respectively. Whereas the wild type and MI6 strains exhibit similar NADP$^+$/NADPH ratios, FS1 contained a significantly more oxidized NADP pool. As the NADP$^+$/NADPH ratio is expected to depend on the PSI/PSII content, we measured the PSI/PSII ratios in the thylakoids by EPR (39). The ratios were found to be similar in the three strains in the 2.5–2.9 range (data not shown).

Purification of an FNR$_L$-PC Complex—To study FNR$_L$ under conditions as close as possible to its native conformation, we purified an FNR$_L$-PBS subcomplex from CBH, a *Synechocystis* mutant that contained a His tag in FNR$_L$ (Fig. 1). The tag had no effect on either the cell growth characteristics or its PBS composition (data not shown).

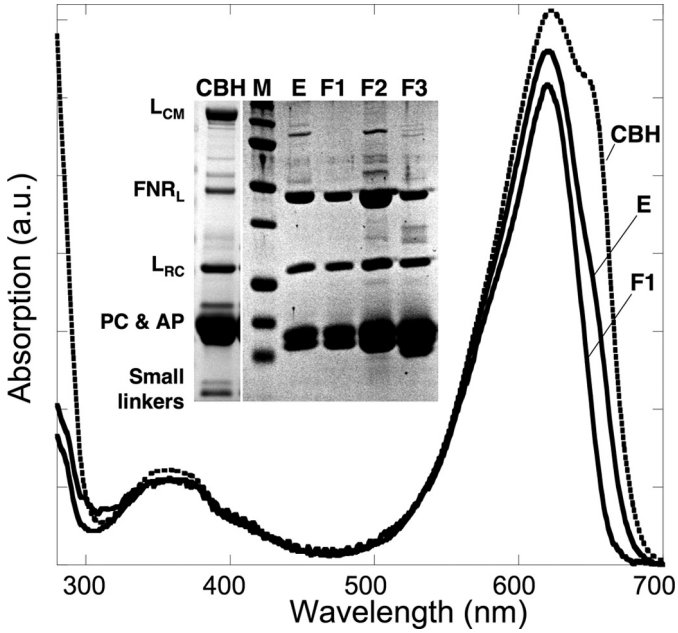

FIGURE 2. **Purification of the FNR$_L$-PC complex.** Absorption spectra of sample fractions during the purification steps, CBH: PBS preparation (*dotted line*) where AP (λ_{max}, 650 nm) and PC (λ_{max}, 620 nm) peaks are visible, *E*, the sample after Ni-affinity chromatography contains PC and a shoulder at 650 nm due to traces of AP; *F1*, the major fraction from gel filtration chromatography exhibits a PC spectrum with a shoulder at 580 nm indicating the presence of L$_{RC}$. The polypeptide composition of the samples was analyzed by SDS-PAGE. *Inset*, CBH; *M*, molecular markers, *E1*, after Ni-affinity chromatography; *F1*, first and major fraction; *F2* and *F3*, minor fractions from gel filtration chromatography. The identities of the polypeptides are indicated on the *left*.

Fig. 2 illustrates the purification protocol as followed both by UV/visible absorption spectroscopy and by SDS-PAGE. The specific absorption of the PBS starting material at 650 nm (AP contribution) strongly decreases during the different purification steps (PBS gradient, Ni-affinity chromatography, and gel filtration). Denaturing electrophoresis clearly shows an enrichment of FNR$_L$ after the Ni-column (*lane E*) but the complex contained minor impurities that are ascribed to L$_{CM}$ (the core membrane linker of the phycobilisome) and AP subunits as evidenced by the shoulder at 650 nm in the corresponding spectrum. The impurities were then eliminated from FNR$_L$-PC by gel filtration. Indeed only Fraction F1 corresponds to pure FNR$_L$-PC as it contained only FNR$_L$, α^{PC}, β^{PC}, and L$_{RC}$, as observed by SDS-PAGE (Fig. 2, *lane F1*). The molecular mass of FNR$_L$-PC was determined to be 330 kDa. F2 and F3 are minor fractions of lower molecular weight (supplemental Fig. S1).

The polypeptide composition of the purified FNR$_L$-PC was evaluated by densitometry of the Coomassie Blue-stained SDS-PAGE bands and indicates that the protein partners, FNR$_L$: L$_{RC}$: $(\alpha^{PC},\beta^{PC})_6$, are in a 1:1:1 stoichiometry. The estimated mass of the complex (330 kDa) closely matches its theoretical mass (303 kDa), which takes into account one phycocyanin hexamer (229 kDa) binding one FNR$_L$ (46 kDa) and one L$_{RC}$ (28 kDa). A direct measurement of the FAD content at 461 nm was impossible due to the large PC absorption. Therefore, an extraction procedure was applied (see "Experimental Procedures" and supplemental Fig. S2), leading to an occupancy value from 92 to 100% for the FAD cofactor in FNR$_L$-PC (Table 1).

TABLE 1

Quantification of FNR$_L$ and FAD in FNR$_L$-PC

Three different FNR$_L$-PC samples have been trichloroacetic acid precipitated, and analyzed for their FNR$_L$ and FAD contents. For each sample, the result is an average of three measurements. Taking together the results of the three samples, one gets a [FAD]/[FNR$_L$] ratio of between 0.92 and 1.00.

Sample	FNR$_L$ concentration	FAD concentration	[FAD]/[FNR$_L$]
	μM	μM	
A	0.43 ± 0.02	0.39 ± 0.02	0.91 ± 0.09
B	0.55 ± 0.04	0.49 ± 0.05	0.89 ± 0.16
C	1.22 ± 0.03	1.19 ± 0.04	0.98 ± 0.06

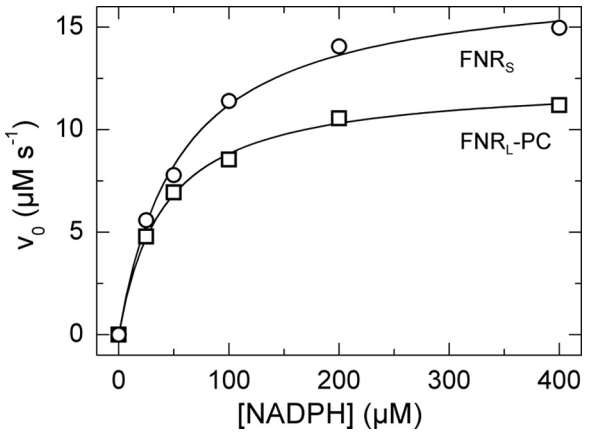

FIGURE 3. **Ferricyanide reductase activities of FNR$_S$ and FNR$_L$-PC.** $K_3[Fe(CN)_6]$ was premixed with 0.025–0.1 μM FNR$_{S/L}$ in 150 mM KP pH 8 and 5 mM $MgCl_2$ at room temperature. The reaction was started by addition of 25–400 μM NADPH. For the FNR$_L$-PC preparation, at least two measurements have been carried out at each given point. The data were normalized to an FNR$_{S/L}$ concentration of 0.1 μM and were fitted with the Henri-Michaelis-Menten equation: For FNR$_S$ (*open circles*) and FNR$_L$-PC (*open squares*), $K_{m(NADPH)}$ values were 55 ± 5 μM and 40 ± 3 μM, respectively. The turnover number k_{cat} for FNR$_S$ and FNR$_L$-PC were 174 ± 5 s^{-1} and 124 ± 3 s^{-1}, respectively.

It has been recently reported that two types of PBS could be found in *Synechocystis*, the conventional one that contains L$_{RC1}$ encoded by *cpcG1* and another one that lacks the core substructure and contains the *cpcG2* encoded L$_{RC2}$ (40, 41). We analyzed the L$_{RC}$ polypeptide contained in the FNR$_L$-PC complex by MALDI-TOF mass spectrometry, and this polypeptide was identified as L$_{RC1}$.

Ferricyanide Reductase Activity—NADPH oxidase activity (also called diaphorase activity) was used to measure the FNR turnover and its affinity for NADPH, in the presence of the artificial electron acceptor potassium ferricyanide. The diaphorase reaction starts with binding of NADPH to FNR, which is followed by the formation of a charge-transfer complex and then hydride transfer from NADPH to FAD (42). Electrons are then transferred to ferricyanide in a non-rate-limiting one-electron reaction. Initial enzyme velocities were plotted as a function of NADPH concentration and fitted according to the Henri-Michaelis-Menten equation (Fig. 3). Both $K_{m(NADPH)}$ and k_{cat} were found to be 30% smaller in FNR$_L$-PC than in FNR$_S$, which results in similar catalytic efficiencies (Table 2).

Ferredoxin-mediated Cytochrome c Reductase Activity—This NADPH oxidase activity was used to measure the affinity for Fd and the turnover of FNR in the presence of its natural electron acceptor Fd. After hydride transfer from NADPH to FNR, electrons flow to Fd, which is then reoxidized by cyt *c*. To obtain specific information about the Fd reduction step, the initial enzyme velocities were obtained by varying the amount of Fd under saturating concentrations of NADPH and cyt *c*. The initial rates of cyt *c* reduction were plotted as a function of Fd concentrations (Fig. 4) and fitted after the Henri-Michaelis-Menten equation. Table 2 highlights the similarities and differences between the two FNR isoforms: similar k_{cat} values in both isoforms, $K_{m(Fd)}$ 70% larger and catalytic efficiency 44% smaller in FNR$_L$-PC than in FNR$_S$ were found.

Single Electron Transfer from Reduced Ferredoxin—The kinetics of FNR reduction in the ternary mixture PSI/Fd/FNR were measured by flash absorption spectroscopy (5). After the actinic flash has triggered a charge separation in PSI, an electron transfer cascade is occurring toward FNR, via Fd. The

TABLE 2

Catalytic properties of the FNR$_L$-PC and FNR$_S$ isoforms

FNR catalytic properties (unit)	FNR$_L$-PC	FNR$_S$
Ferricyanide reductase activity		
$K_{m(NADPH)}$ (μM)	40 ± 3	55 ± 5
k_{cat} (s^{-1})	124 ± 3	174 ± 5
k_{cat}/K_m (μM^{-1}s^{-1})	3.1 ± 0.3	3.2 ± 0.4
Cytochrome c reductase activity		
$K_{m(Fd)}$ (μM)	47 ± 6	28 ± 2
k_{cat} (s^{-1})	144 ± 12	154 ± 6
k_{cat}/K_m (μM^{-1}s^{-1})	3.1 ± 0.7	5.5 ± 0.6
Single reduction of FNR by Fd$_{red}$		
no NADP$^+$		
Second-order forward rate k_1 (μM^{-1}s^{-1})	14.1	24.9
Second-order reverse rate k_{-1} (μM^{-1}s^{-1})	4.6	10.6
$K_{eq} = k_1/k_{-1}$	3.06	2.35
$E_{m(FNRox/FNRsq)}$[a] (mV)	−384	−390
1 mM NADP$^+$		
Second-order forward rate k_1 (μM^{-1}s^{-1})	10.8	15.2
Second-order reverse rate k_{-1} (μM^{-1}s^{-1})	4.0	5.4
$K_{eq} = k_1/k_{-1}$	2.73	2.84
$E_{m(FNRox/FNRsq)}$[a] (mV)	−386	−385
Multiple turnover: Initial rate of reoxidation of 3.75 μM Fd$_{red}$ (reoxidized Fd$_{red}$ per second and per FNR)		
Observed rate	50	53/(330)[b]
Calculated rate (with limiting k_1)	40.5	57/(1564)[b]

[a] Vs NHE. Calculated assuming $E_{m(Fdox/Fdred)} = -412$ mV (44).

[b] Numbers in italics were obtained at low ionic strength and recalculated from Ref. 5 by using an absorption coefficient of 9,000 M^{-1}cm^{-1} for FNR$_S$ at 461 nm instead of 10,800 M^{-1}cm^{-1} (giving *e.g.* k_1 = 417 μM^{-1}s^{-1}).

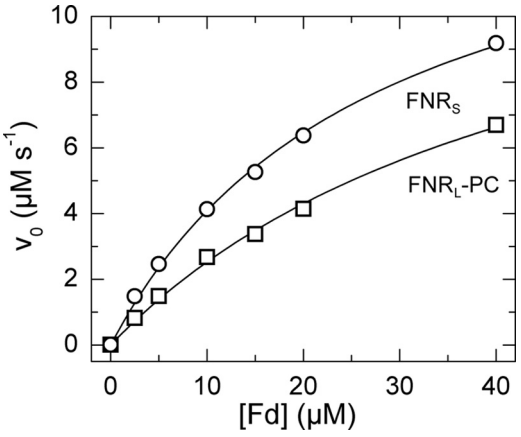

FIGURE 4. **Fd-mediated cyt *c* reductase activities of FNR$_S$ and FNR$_L$-PC.** FNR$_{L/S}$ was mixed with 2.5–40 μM Fd from *T. elongatus* and 40 μM cyt *c* in 150 mM KP buffer pH 8 at 25 °C. The reaction was started by injection of 400 μM NADPH. The data were normalized to an FNR$_{S/L}$ concentration of 0.1 μM. For FNR$_S$ (*open circles*) and FNR$_L$-PC (*open squares*), the $K_{m(Fd)}$ values were 28 ± 2 μM and 47 ± 6 μM, respectively. The turnover number k_{cat} for FNR$_S$ and FNR$_L$-PC were 154 ± 6 s^{-1} and 144 ± 12 s^{-1}, respectively.

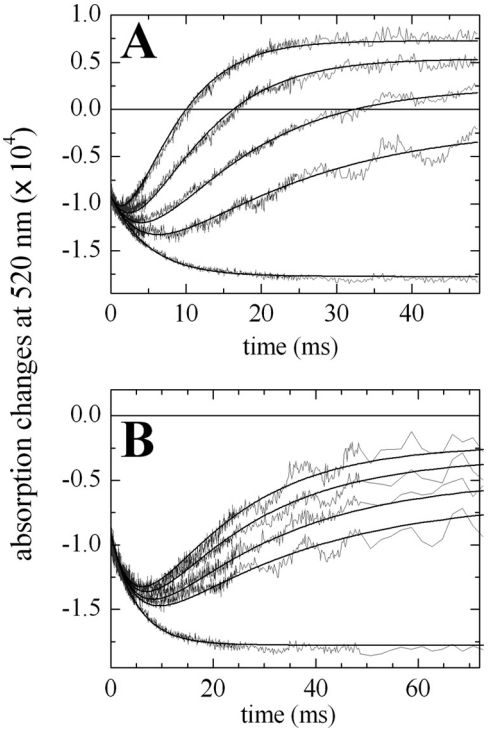

FIGURE 5. **Flash titration of FNR$_S$ and FNR$_L$-PC in the presence of 1 mM NADP$^+$ under single reduction conditions.** The absorption changes at 520 nm are attributed to electron acceptors as the P700$^+$ formation and decay have been subtracted. The *solid line* at zero level corresponds to the baseline before the flash. Concentrations of PSI and Fd were 0.475 μM and 3.96 μM. *A*, concentrations of FNR$_S$ were 0, 2.0, 4.0, 8.0, and 16.0 μM for curves from *bottom to top*. The best fit resulted in k_r = 50 μM^{-1} s^{-1}, k_1 = 15.2 μM^{-1} s^{-1}, and k_{-1} = 5.4 μM^{-1} s^{-1}. *B*, concentrations of FNR$_L$-PC were 0, 1.6, 2.1, 3.0, and 3.7 μM for curves from *bottom to top*. The best fit resulted in k_r = 50 μM^{-1} s^{-1}, k_1 = 10.8 μM^{-1} s^{-1}, and k_{-1} = 4.0 μM^{-1} s^{-1}.

measurements were performed in the absence/presence of NADP$^+$ and, in order to favor single FNR reduction, FNR was in large excess over PSI (and therefore over photoreduced Fd). The kinetics in the presence of 1 mM NADP$^+$ are shown in Fig. 5*A* for different FNR$_S$ concentrations, together with a control experiment without FNR$_S$. The signals are only due to reduction of the PSI electron acceptors, Fd and FNR as the P700$^+$ contribution has been eliminated (see "Experimental Procedures"). In the control experiment (bottom trace), two different kinetic components are present. The fastest component is not time resolved and is attributed to the formation of the reduced PSI terminal acceptor $(F_A, F_B)^-$, as confirmed by a sample without Fd (data not shown). A very small and fast submicrosecond to microsecond signal due to Fd reduction (<10% of the full Fd reduction signal) was observed, corresponding to a small amount of PSI:Fd complex present before flash excitation (data not shown; see also Ref. 43). This is in line with the large dissociation constant K_d that is expected for the PSI:Fd complex under our conditions (150 mM potassium phosphate, pH 8). The slowest millisecond absorption decrease is due to Fd reduction by a second-order diffusion-limited process. In the presence of FNR$_S$, the same initial fast decay is observed but a signal increase, which is ascribed to the reduction of FNR$_S$ by Fd$_{red}$, dominates the subsequent absorption changes. The rates and the final amplitudes of this signal increase when FNR$_S$ concentration increases. The kinetic model we used to simulate the observed kinetics is shown in Reactions 1 and 2.

$$PSI_{red} + Fd_{ox} \xrightarrow{k_r} PSI_{ox} + Fd_{red}$$

REACTION 1

$$Fd_{red} + FNR_{ox} \underset{k_{-1}}{\overset{k_1}{\rightleftharpoons}} Fd_{ox} + FNR_{sq}$$

REACTION 2

In Reaction 1, PSI$_{red}$ stands for PSI with the terminal acceptor (F_A, F_B) reduced. Reduction of (F_A, F_B) occurs in the submicrosecond time range and thus does not need to be considered. This kinetic model can be analytically solved in a simplified version when all reactions are considered as pseudo first-order (see "Experimental Procedures" for the solution equations). This allowed us to perform a global fit analysis resulting in the following values: k_r = 50.0 μM^{-1} s^{-1}, k_1 = 15.2 μM^{-1} s^{-1}, k_{-1} = 5.4 μM^{-1} s^{-1}. The redox equilibrium constant K_{eq} = 2.84 can be calculated for Reaction 2 (k_1/k_{-1}). This constant is related to the difference in midpoint redox potentials (E_m) of the reaction partners in Equation 11.

$$\Delta E_m = E_{m(FNR_{ox}/FNR_{sq})} - E_{m(Fd_{ox}/Fd_{red})} = (RT/F)\ln(K_{eq}) \quad \text{(Eq. 11)}$$

Assuming E_m = −412 mV for *Synechocystis* Fd (44), one gets −385 mV for $E_{m(FNRox/FNRsq)}$, which is very close to the value of −382 mV previously determined under conditions of moderate ionic strength (30 mM NaCl, 5 mM $MgCl_2$; the value of −378 mV in Ref. 5 has been recalculated using $\epsilon_{461\ nm}$ = 9,000 M^{-1} cm^{-1} for FNR). It should be noted that measuring $E_{m(FNRox/FNRsq)}$ by standard methods is fairly difficult because the thermodynamically unstable semiquinone (45) is only marginally observed during a redox titration.

The same experiment was performed with FNR$_L$-PC and the corresponding kinetics are shown in Fig. 5*B*. Fitting these data gave similar values of K_{eq} and hence of $E_{m(FNRox/FNRsq)}$, whereas the second-order rate constants were 25–30% smaller than with FNR$_S$ (Table 2). The smaller rate constants measured with FNR$_L$-PC are in accordance with its larger $K_{m(Fd)}$ observed in the ferredoxin-mediated cyt *c* reduction assay. The above experiments were repeated in the absence of NADP$^+$, to compare the kinetics in the presence or absence of a ternary complex Fd/FNR/NADP$^+$. These results are summarized in Table 2: For both isoforms the E_m is very similar to those measured in the presence of NADP$^+$. This indicates that the electrostatic environment of FAD is not modified by NADP$^+$. In contrast, the k_1 and k_{-1} rates are larger in the absence of NADP$^+$, in agreement with a previous study, where this effect was attributed to a repulsive electrostatic effect between the phosphate moiety of NADP$^+$ and the negatively charged Fd (5).

Catalytic Turnover of the Two FNR Isoforms during NADP$^+$ Reduction—We also measured FNR-reduction kinetics obtained for a ternary mixture PSI/Fd/FNR in the presence of

$NADP^+$ under multiple catalytic turnover conditions (5). These conditions were met by using PSI in large excess over FNR (3.75 μM *versus* 0.15/0.3 μM). Fd (8 μM) is also added in excess over PSI so that Fd_{red}, at a PSI equivalent concentration, is rapidly formed after PSI photoexcitation. Fd_{red} is then slowly monoexponentially reoxidized by FNR (rate k_{FNR}). Taking into account the decay without FNR (rate $k_{no\ FNR}$), we obtained values of 2.2 and 4.1 s^{-1} for ($k_{FNR} - k_{no\ FNR}$) with 0.15 and 0.30 μM FNR_S, respectively. This corresponds to 55 and 51 reoxidized Fd_{red} per second and per FNR_S, respectively and the average value of 53 is indicated in Table 2. Using the same enzyme concentrations, the ($k_{FNR} - k_{no\ FNR}$) rates are quite similar to those of FNR_L-PC (2.14 and 3.69 s^{-1}). This corresponds to an averaged value of 50 reoxidized Fd_{red} per second and per FNR_L-PC (Table 2). Overall, the multiple turnover rates are similar for the two isoforms.

As the second-order rate constants k_1 measured for the first FNR reduction are rather small under our conditions (see "Discussion"), it is worth checking if this process could be rate limiting during the catalysis (see Equation 10 under "Experimental Procedures"). The similarity between the calculated and measured turnover rates (Table 2) indicates that this is indeed the case. Thus we have identified under our conditions a limiting step which has not been identified previously. As a control, we also considered FNR_S under low ionic strength conditions (5) in order to compare the measured and calculated turnovers (bracketed values in Table 2). The 5-fold excess in calculated *versus* measured turnover shows that in this case of faster turnover, FNR_S reduction by Fd_{red} is not rate limiting.

DISCUSSION

Based on the observation that in *Synechocystis* FNR_S accumulates only under heterotrophic or starvation conditions whereas FNR_L is the major isoform detected under photoautotrophic conditions (24), it was proposed that each isoform plays a specific role. In this work, we have shown that under photoautotrophic conditions the $NADP^+$/NADPH ratio is higher in a mutant containing only FNR_S. Furthermore this observation cannot be attributed to a different PSI/PSII ratio as the ratio was shown to be unchanged in FS1 compared with that of the wild type. This reinforces the hypothesis that the FNR isoforms have different roles. FS1 seems unable to accumulate the NADPH amounts produced in the strains (wild type and MI6) where FNR_L is the main isoform. This also explains the fact that photoautotrophic growth is impaired in FS1, while MI6 growth is similar to that of the wild type (24). We decided to check whether the *in vivo* differences could be explained by the *in vitro* properties of the two FNR isoforms. In other words, is there any selectivity of the two isolated FNR isoforms for $NADP^+$ reductase *versus* NADPH oxidase activities? Such a selectivity has been observed in the case of root and leaf FNR isoforms in plants (3, 12, 14–17, 46).

Purification of an L_{RC}-containing FNR_L:PC Complex—The best compromise between approaching the *in vivo* situation and feasibility (stability, compatibility with absorption-spectroscopy studies) was to obtain a PBS subcomplex containing FNR_L and a PC hexamer $(\alpha^{PC}, \beta^{PC})_6$. The purification was facilitated by a His tag in the hinge domain of FNR_L. We obtained a pure and homogeneous complex, as judged by gel filtration, SDS-PAGE analysis, and FAD content. The stoichiometry of FNR_L:L_{RC}:$(\alpha^{PC}, \beta^{PC})_6$ in the 300-kDa complex was found to be 1:1:1. Furthermore it was verified that the L_{RC} polypeptide present in FNR_L-PC was encoded by *cpcG1*, which was expected since conventional PBS were used for its purification. It was recently proposed, using single particle analysis of CBH PBS, that FNR_L is located at the interface between the rod and the core (22). From our purification data, it can be further concluded that FNR_L is bound at only one of the PC hexamers, with no major involvement of the other hexamers. The complex was stable, for at least 2 weeks at 4 °C, with no proteolysis of FNR_L. This is probably due to protection of the FNR_L linker-domain by the PC hexamer.

Effect of High Ionic Strength on the Catalytic Properties of FNR_S—With the aim of comparing FNR_S and FNR_L-PC, we performed a broad set of measurements on NADPH-oxidase and $NADP^+$-reductase activities of the two isoforms as summarized in Table 2. These measurements were performed under high ionic strength conditions (150 mM potassium phosphate) because such conditions are necessary to stabilize the FNR_L-PC complex. We compared our data to those previously obtained for cyanobacterial FNR_S at lower ionic strength. The NADPH-oxidase catalytic parameters (measured via ferricyanide reduction) are quite similar to those previously reported for FNR_S from *Anabaena* sp. (k_{cat} 20% smaller, $K_{m(NADPH)}$ about 2-fold greater in our case; Ref. 47). This implies that this ionic strength is not detrimental for diaphorase activity. Regarding the ferredoxin-mediated NADPH-oxidase activity, we found a 3-fold increase in $K_{m(Fd)}$ and only a 25% decrease in k_{cat}, between our measurements and those previously measured in the same report with *Anabaena* FNR_S (47). The $K_{m(Fd)}$ increase can be attributed to the screening of electrostatic interactions occurring at high ionic strength between FNR and Fd (2). A similar screening effect explains our data concerning FNR_S reduction by Fd_{red} when compared with a previous study, conducted under lower ionic strength (5): the second-order rate constant k_1 of single FNR_S reduction by Fd_{red} is 28-fold smaller and during multiple turnover, the rate of Fd_{red} reoxidation is 6 times smaller in the present study. We also obtained evidence that at high ionic strength, k_1 is rate limiting during multiple turnover, which is not the case at lower ionic strength. Under these last conditions, the enzyme turnover is much faster and is limited by one of the first-order processes (Fd_{ox} dissociation, hydride transfer, or NADPH release).

Comparison of the Catalytic Properties of FNR_S and FNR_L-PC: an Analogous System to Leaf and Root FNR Isoforms?—The following catalytic parameters are quite similar for the two *Synechocystis* isoforms: the catalytic efficiency (k_{cat}/K_m) of NADPH/ferricyanide oxidoreduction, the k_{cat} of the Fd-mediated cyt *c* reduction, the E_m (FNR_{ox}/FNR_{sq}) in the presence/absence of $NADP^+$ and the initial reoxidation rate of Fd_{red} by FNR during multiple catalytic turnover. Differences between the two isoforms were observed: 30% smaller K_m(NADPH) and k_{cat} of FNR_L-PC *versus* FNR_S during NADPH/ferricyanide oxidoreduction, a 70% larger $K_{m(Fd)}$ and a 44% smaller catalytic efficiency of FNR_L-PC for the Fd-mediated cyt *c* reductase activity, and a 29/43% ($NADP^+$ present/absent) decrease in k_1,

the rate of single FNR reduction by Fd_{red}, for FNR_L-PC (Table 2). The slight decrease in $K_{m(NADPH)}$ and k_{cat} during ferricyanide reduction indicates that the presence of the PC hexamer slightly modifies the association of NADPH to FNR and/or the following steps leading to FAD reduction. The increase in $K_{m(Fd)}$ and the decrease in k_1 are likely due to a steric hindrance by, or a conformational effect due to, the PC hexamer moiety of FNR_L-PC. We favor these explanations over electrostatic repulsion brought by PC, because electrostatic interactions are expected to be of limited importance at high ionic strength. Moreover, the electrostatic environment of FAD appears to be unmodified in FNR_L-PC as judged by the similar $E_{m(FNRox/FNRsq)}$ measured for the two isoforms. Overall, the results obtained for the Fd-mediated cyt *c* reductase activity are in agreement with the different predicted roles for the FNR isoforms. Both isoforms are capable of catalyzing $NADP^+$ reduction under multiple turnover conditions. Furthermore, we obtained indications that in our conditions electron transfer from Fd_{red} is rate limiting.

The leaf and root FNR isoforms from plants differ mainly in four catalytic or thermodynamic parameters (supplemental Table S1): 1) $K_{m(NADPH)}$, measured via ferricyanide reduction, is 3–10-fold higher, depending on the authors, for leaf FNR compared with root FNR (14, 16). We observed a 30% decrease in FNR_L-PC *versus* FNR_S. If we tentatively make the parallel between FNR_L-PC and leaf FNR on the one hand, and between FNR_S and root FNR on the other hand, the situation seems reversed; 2) $K_{m(leaf\ Fd)}$, measured by Fd-mediated cyt *c* reduction, is 5–10-fold smaller for leaf FNR than for to root FNR (3, 14, 17, 46). The 70% difference that we observe is also in the unexpected direction; 3) k_{cat} of the Fd-mediated cyt *c* reduction is 3–4-fold smaller for leaf FNR than for root FNR (3, 14, 17, 46). We observed no significant difference in this parameter; 4) The $E_{m(FNRox/FNRred}$ couple, 2-electron reduction) of corn root FNR is 20 mV higher than the midpoint potential of spinach leaf FNR (15). Unfortunately, no comparison is available for two FNR isoforms from the same plant, to our knowledge. We observed no significant difference for $E_{m(FNRox/FNRsq)}$ between the two *Synechocystis* isoforms.

Contrary to the case of *Synechocystis*, there are some differences in the catalytic domains of the plant FNR isoforms. Moreover, the existence of Fd isoforms is essential when comparing the processes of $NADP^+$ reduction and NADPH oxidation in leaves and roots. The E_m of root Fd was found to be much higher than that of leaf Fd (50–100 mV difference; Refs 17, 46, 48, 49). This probably favors NADPH oxidation in roots *versus* $NADP^+$ reduction in leaves. Many different Fd encoding genes have been identified in *Synechocystis* (50). In the present work we studied the major Fd encoded by *fed1*. This Fd shares with the leaf Fd a similar redox potential but both root and leaf Fds appear to be phylogenetically equally distant to the *Synechocystis* Fd (17). At our present state of knowledge, there is no equivalent of the root Fd in cyanobacteria, in terms of redox potential, and the major photosynthetic Fd is generally thought to be involved in all bioenergetically significant electron flows. This was also a basic assumption in our approach. However, the involvement of other Fd isoforms under heterotrophic conditions cannot be excluded.

CONCLUSION

From recent data (24), specific roles were proposed for the two *Synechocystis* FNR isoforms, which seem to parallel the enzymatic selectivity of plant FNR root and leaf isoforms. Such specificity is also supported by the change in the $NADP^+$/NADPH ratios that we measured in *Synechocystis* cells containing only one of the isoforms. However, from a detailed functional characterization, we observed small differences in the $NADP^+$ reductase and NADPH oxidase activities of FNR_S and FNR_L-PC complex. This contrasts with the much larger *in vitro* differences observed between leaf and root FNR isoforms from plants.

If the main photosynthetic Fd (50) is involved *in vivo* in electron transfer with both isoforms (see above), the differences that we observe might not fully explain the *in vivo* properties of the *Synechocystis* mutants expressing only one of the isoforms. Besides the intrinsic catalytic properties of those isoforms, it would be necessary to invoke their localization or association to other complexes. For example, it can be speculated that FNR_S is involved in cyclic/respiratory electron flow because it is free to bind to other membrane complexes such as NADPH dehydrogenase or cytochrome b_6f. Conversely, PBS-bound FNR_L cannot play such a role and is therefore dedicated to $NADP^+$ photoreduction. For both types of activities, substrates availability (Fd_{red}/Fd_{ox} and $NADP^+$/NADPH) might also be key *in vivo* characteristics for the activity of the two isoforms. This situation would be reminiscent of what has been described recently for the different leaf isoforms, where catalytic activities appear to depend upon their variable attachment to the thylakoid membrane (51, 52).

In this context, it would be worth studying the involvement of CpcG2-PBS, which lacks the PBS core, in binding FNR_L, as it has been hypothesized to be directly bound to PSI (53). However the small amount of CpcG2-PBS *versus* CpcG1-PBS in the wild type (40) and the effect of cpcG2 disruption on the PSI/PSII ratio (41) are obstacles, which have to be surmounted for such studies. Further *in vivo* measurements are needed to better understand the reason for which FNR binds the PBS in the majority of PBS-containing cyanobacteria.

Acknowledgments—We thank V. Mary for skillful technical assistance and Dr. F. Haraux for discussions. C. Bordot is acknowledged for initial work on the His-tagged complex and Dr. A. Boussac for the gift of T. elongatus soluble extracts. We thank C. Deladriere and A. Guillot (PAPPSO, Jouy-en-Josas) for mass spectroscopy analysis.

REFERENCES

1. Batie, C. J., and Kamin, H. (1984) *J. Biol. Chem.* **259,** 11976–11985
2. Hurley, J. K., Morales, R., Martínez-Júlvez, M., Brodie, T. B., Medina, M., Gómez-Moreno, C., and Tollin, G. (2002) *Biochim. Biophys. Acta* **1554,** 5–21
3. Hanke, G. T., Kurisu, G., Kusunoki, M., and Hase, T. (2004) *Photosynth. Res.* **81,** 317–327
4. Karplus, P. A., and Faber, H. R. (2004) *Photosynth. Res.* **81,** 303–315
5. Cassan, N., Lagoutte, B., and Sétif, P. (2005) *J. Biol. Chem.* **280,** 25960–25972
6. Bruns, C. M., and Karplus, P. A. (1995) *J. Mol. Biol.* **247,** 125–145
7. Carrillo, N., and Ceccarelli, E. A. (2003) *Eur. J. Biochem.* **270,** 1900–1915
8. Batie, C. J., and Kamin, H. (1984) *J. Biol. Chem.* **259,** 8832–8839

9. Forti, G., and Sturani, E. (1968) *Eur. J. Biochem.* **3,** 461–472
10. Morigasaki, S., Takata, K., Suzuki, T., and Wada, K. (1990) *Plant Physiol.* **93,** 896–901
11. Okutani, S., Hanke, G. T., Satomi, Y., Takao, T., Kurisu, G., Suzuki, A., and Hase, T. (2005) *Plant Physiol.* **139,** 1451–1459
12. Gummadova, J. O., Fletcher, G. J., Moolna, A., Hanke, G. T., Hase, T., and Bowsher, C. G. (2007) *J. Exp. Bot.* **58,** 3971–3985
13. Green, L. S., Yee, B. C., Buchanan, B. B., Kamide, K., Sanada, Y., and Wada, K. (1991) *Plant Physiol.* **96,** 1207–1213
14. Onda, Y., Matsumura, T., Kimata-Ariga, Y., Sakakibara, H., Sugiyama, T., and Hase, T. (2000) *Plant Physiol.* **123,** 1037–1045
15. Aliverti, A., Faber, R., Finnerty, C. M., Ferioli, C., Pandini, V., Negri, A., Karplus, P. A., and Zanetti, G. (2001) *Biochemistry* **40,** 14501–14508
16. Aliverti, A., Pandini, V., and Zanetti, G. (2004) *Biochim. Biophys. Acta* **1696,** 93–101
17. Hanke, G. T., Kimata-Ariga, Y., Taniguchi, I., and Hase, T. (2004) *Plant Physiol.* **134,** 255–264
18. Schluchter, W. M., and Bryant, D. A. (1992) *Biochemistry* **31,** 3092–3102
19. Glazer, A. N. (1989) *J. Biol. Chem.* **264,** 1–4
20. van Thor, J. J., Gruters, O. W., Matthijs, H. C., and Hellingwerf, K. J. (1999) *EMBO J.* **18,** 4128–4136
21. Gómez-Lojero, C., Pérez-Gómez, B., Shen, G. Z., Schluchter, W. M., and Bryant, D. A. (2003) *Biochemistry* **42,** 13800–13811
22. Arteni, A. A., Ajlani, G., and Boekema, E. J. (2009) *Biochim. Biophys. Acta* **1787,** 272–279
23. van Thor, J. J., Jeanjean, R., Havaux, M., Sjollema, K. A., Joset, F., Hellingwerf, K. J., and Matthijs, H. C. P. (2000) *Biochim. Biophys. Acta* **1457,** 129–144
24. Thomas, J. C., Ughy, B., Lagoutte, B., and Ajlani, G. (2006) *Proc. Natl. Acad. Sci. U.S.A.* **103,** 18368–18373
25. Nakajima, M., Sakamoto, T., and Wada, K. (2002) *Plant Cell Physiol.* **43,** 484–493
26. Ughy, B., and Ajlani, G. (2004) *Microbiology* **150,** 4147–4156
27. Rögner, M., Nixon, P. J., and Diner, B. A. (1990) *J. Biol. Chem.* **265,** 6189–6196
28. Barth, P., Guillouard, I., Sétif, P., and Lagoutte, B. (2000) *J. Biol. Chem.* **275,** 7030–7036
29. Gantt, E., and Lipschultz, C. A. (1972) *J. Cell Biol.* **54,** 313–324
30. Elmorjani, K., Thomas, J. C., and Sebban, P. (1986) *Arch. Microbiol.* **146,** 186–191
31. Ajlani, G., Vernotte, C., DiMagno, L., and Haselkorn, R. (1995) *Biochim. Biophys. Acta* **1231,** 189–196
32. Glazer, A. N. (1985) *Annu. Rev. Biophys. Chem.* **14,** 47–77
33. Engel, P. C., and Massey, V. (1971) *Biochem. J.* **125,** 879–887
34. Whitby, L. G. (1953) *Biochem. J.* **54,** 437–442
35. Shin, M. (1971) *Methods Enzymol.* **23,** 440–447
36. Zanetti, G., and Arosio, P. (1980) *FEBS Lett.* **111,** 373–376
37. Sétif, P., Fischer, N., Lagoutte, B., Bottin, H., and Rochaix, J. D. (2002) *Biochim. Biophys. Acta* **1555,** 204–209
38. Brettel, K., and Leibl, W. (2001) *Biochim. Biophys. Acta* **1507,** 100–114
39. Danielsson, R., Albertsson, P. A., Mamedov, F., and Styring, S. (2004) *Biochim. Biophys. Acta* **1608,** 53–61
40. Kondo, K., Geng, X. X., Katayama, M., and Ikeuchi, M. (2005) *Photosynth. Res.* **84,** 269–273
41. Kondo, K., Ochiai, Y., Katayama, M., and Ikeuchi, M. (2007) *Plant Physiol.* **144,** 1200–1210
42. Tejero, J., Peregrina, J. R., Martínez-Júlvez, M., Gutiérrez, A., Gómez-Moreno, C., Scrutton, N. S., and Medina, M. (2007) *Arch. Biochem. Biophys.* **459,** 79–90
43. Sétif, P. Q., and Bottin, H. (1994) *Biochemistry* **33,** 8495–8504
44. Bottin, H., and Lagoutte, B. (1992) *Biochim. Biophys. Acta* **1101,** 48–56
45. Corrado, M. E., Aliverti, A., Zanetti, G., and Mayhew, S. G. (1996) *Eur. J. Biochem.* **239,** 662–667
46. Gou, P., Hanke, G. T., Kimata-Ariga, Y., Standley, D. M., Kubo, A., Taniguchi, I., Nakamura, H., and Hase, T. (2006) *Biochemistry* **45,** 14389–14396
47. Medina, M., Martinez-Júlvez, M., Hurley, J. K., Tollin, G., and Gómez-Moreno, C. (1998) *Biochemistry* **37,** 2715–2728
48. Aliverti, A., Hagen, W. R., and Zanetti, G. (1995) *FEBS Lett.* **368,** 220–224
49. Akashi, T., Matsumura, T., Ideguchi, T., Iwakiri, K., Kawakatsu, T., Taniguchi, I., and Hase, T. (1999) *J. Biol. Chem.* **274,** 29399–29405
50. Poncelet, M., Cassier-Chauvat, C., Leschelle, X., Bottin, H., and Chauvat, F. (1998) *Mol. Microbiol.* **28,** 813–821
51. Palatnik, J. F., Valle, E. M., and Carrillo, N. (1997) *Plant Physiol.* **115,** 1721–1727
52. Hanke, G. T., Endo, T., Satoh, F., and Hase, T. (2008) *Plant Cell Environ.* **31,** 1017–1028
53. Kondo, K., Mullineaux, C. W., and Ikeuchi, M. (2009) *Photosynth. Res.* **99,** 217–225